THE JOURNAL OF PHYSICAL CHEMISTRY B
A JOURNAL OF THE AMERICAN CHEMICAL SOCIETY

pubs.acs.org/JPCB

Article

Functional-Group Effect of Ligand Molecules on the Aggregation of Gold Nanoparticles: A Molecular Dynamics Simulation Study

Ayse Cetin* and Mine Ilk Capar

Cite This: J. Phys. Chem. B 2022, 126, 5534−5543

Read Online

ACCESS | Metrics & More | Article Recommendations

ABSTRACT: In this paper, atomistic molecular dynamics simulations are performed for the systems consisting of functionalized gold nanoparticles (NPs) in a toluene medium. Gold NPs are coated with ligand molecules that have different terminal groups, that is, polar carboxyl (COOH), hydroxyl (OH), amine (NH_2), and nonpolar methyl (CH_3). These functional groups are selected to understand the relation between the aggregation behavior of functionalized gold NPs in toluene and the polarity of terminal groups of ligand molecules. The center-of-mass distances between NP pairs, the radial distribution functions, the mean square displacements, the radius of gyration, and the number of hydrogen bonds (H-bond) between ligand molecules are computed. Our simulation results indicate that functionalized gold NPs exhibit different aggregation/dispersion behaviors depending upon the terminal group of ligands.

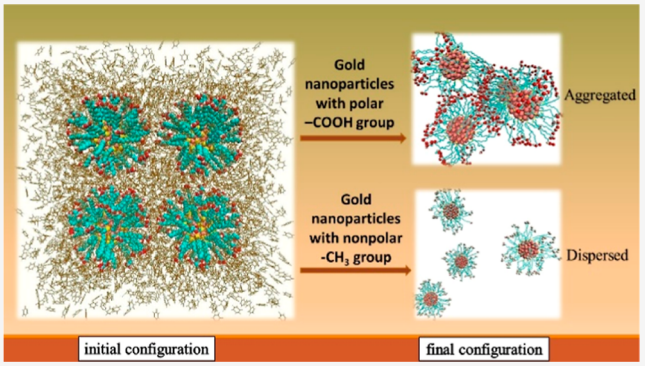

1. INTRODUCTION

Metal nanoparticles (NPs) have several unique physical and chemical properties that cannot be observed in the bulk form of the same materials.[1,2] Gold NPs have become prominent among metal NPs in recent years due to their chemical stability and nontoxic nature. Their ability to be synthesized in various shapes and sizes and their large surface area−volume ratio result in the gold NPs having unique electronic and optical properties. Because of the significant properties of the gold NPs, they are widely used in various fields of application such as sensors, catalysis, drug delivery, photothermal therapy, and biomedical imaging.[3−8] The large surface-area-to-volume ratio of the gold NPs allows us to make surface modifications by coating ligand molecules with different functional groups such as hydrophobic, hydrophilic, cationic, anionic, or neutral groups, thiols, DNA molecules, enzymes, and functional polymers.[9−14] By making surface modifications on the gold NPs, their selectivity to certain surfaces can be improved. The penetration of the particles to the cell membrane is enabled, and they can also carry drugs by holding them on their surfaces.

Depending on the application area, the aggregation or the dispersion of the functionalized gold NPs in a solvent is required. The aggregation of functionalized gold NPs can be the preferred behavior for chemical and biological sensors and also for biomedical imaging applications. On the other hand, it is not desirable behavior in some biological applications such as the injection of functionalized gold NPs into the body for drug delivery. Therefore, determining the factors affecting the aggregation/dispersion behaviors of gold NPs and controlling these behaviors are crucial. Many experimental[15−31] and molecular dynamics (MD) simulation studies[32−51] have been performed to understand the aggregation/dispersion behaviors of functionalized gold NPs. In these simulation studies, the coarse-grained (CG) model[32−43] and realistic atomistic model[44−51] are widely used. There are a few simulation studies that have examined the effect of the polarity of the terminal groups of ligand molecules on the aggregation of functionalized gold NPs.[34,40,46]

Lin et al. have done the CG MD simulations of functionalized gold NPs in water and butane.[34] They examined the effects of ligand terminal chemistry, ligand length, solvents, and temperature. In the water medium, they observed less aggregation behavior with increasing polarity of the functional groups. When butane was used instead of water as an environment, it was observed that gold NPs with alkane terminal groups did not aggregate, while gold NPs with polar terminal groups did. Sridhar et al. performed a CG MD simulation study to understand the effect of surface coverage density and chemistry on the self-assembly of monolayer-protected four gold NPs in water solvents.[40] In addition, the effects of the polar hydroxyl

Received: February 20, 2022
Revised: July 1, 2022
Published: July 15, 2022

https://doi.org/10.1021/acs.jpcb.2c01132
J. Phys. Chem. B 2022, 126, 5534−5543

and nonpolar methyl terminal groups of ligand molecules on the aggregation behavior of functionalized gold NPs in the presence and absence of water were investigated by using atomistic MD simulation by Devi.[46]

According to the literature review, most of the MD simulation studies on understanding the aggregation/dispersion behavior of functionalized gold NPs have been focused on the water medium except for a few studies on butane or ethane media.[34,35] The solvent plays an important role in the aggregation/dispersion process of gold NPs because the interaction between the solvent molecules and ligand molecules affects gold NPs' behaviors and final morphologies. In order to obtain the desired aggregation or dispersion behavior depending on the application area, the appropriate coating and solvent must be selected. From this point of view, we have chosen nonpolar liquid toluene as an environment, which has not been studied before. The toluene solvent is most frequently used as a nonpolar aromatic compound in synthetic organic chemistry and in industrial processes. In this paper, the effect of the polarity of terminal groups of ligand molecules on the aggregation/dispersion of functionalized gold NPs has been investigated in a toluene medium by using atomistic MD simulation. The gold NPs are coated with polar COOH-, OH-, NH_2-, and nonpolar CH_3-terminated alkanethiol ligand molecules. To the best of our knowledge, this is the first MD simulation study in which the toluene medium has been used for understanding the aggregation behavior of functionalized gold NPs.

2. METHODS

In this study, to investigate the aggregation behavior of functionalized gold NPs, atomistic MD simulations are performed using the GROMACS 5.1.4 program.[52] The gold NPs are coated with the $SH(CH_2)_{11}X$ ligand molecules by using the PACKMOL program.[53] Different X terminal groups, which are polar carboxyl (COOH), hydroxyl (OH), amine (NH_2), and nonpolar methyl (CH_3), are used. Optimized coordinates of the gold NPs with 144 Au atoms are taken from the previous work.[54] The Au_{144} NP with a diameter of 2 nm has a nearly spherical rhombicosidodecahedron geometry. It has 30 Au atoms on its surface, 60 atoms are in the lower layer, and the remaining 54 atoms are placed in its center. Each surface Au atom makes a covalent bond with the S atoms of two ligand molecules, that is, S−Au−S. Thus, 30 surface gold atoms are coated with 60 alkylthiol ligands. After coating, four replicated functionalized gold NPs are placed in a rectangular box with the dimensions of nearly 11 × 11 × 6 nm^3. Then, the box is filled with toluene molecules by using GROMACS tools. The numbers of toluene molecules are set in accordance with the experimental density of liquid toluene[55] at the temperature used in this research. By changing ligand molecules as $SH(CH_2)_{11}COOH$ (11-mercaptoundecanoic acid), $SH(CH_2)_{11}OH$ (11-mercapto-1-undecanol), $SH(CH_2)_{11}NH_2$ (11-amino-1-undecanethiol), and $SH(CH_2)_{11}CH_3$ (1-dodecanethiol), four different systems having the same initial conditions are prepared. These are named system I, system II, system III, and system IV, respectively. In each system, the total atom number is approximately 48 000.

The united atom model is used for CH_2 groups in the alkyl chain of ligand molecules and the CH group in the toluene molecule. The schematic representations of ligand molecules and toluene molecules used in this study are given in Figures 1 and 2, respectively. For inter- and intramolecular interactions, the GROMOS force field is used.[56] The potential function of this force field is given by

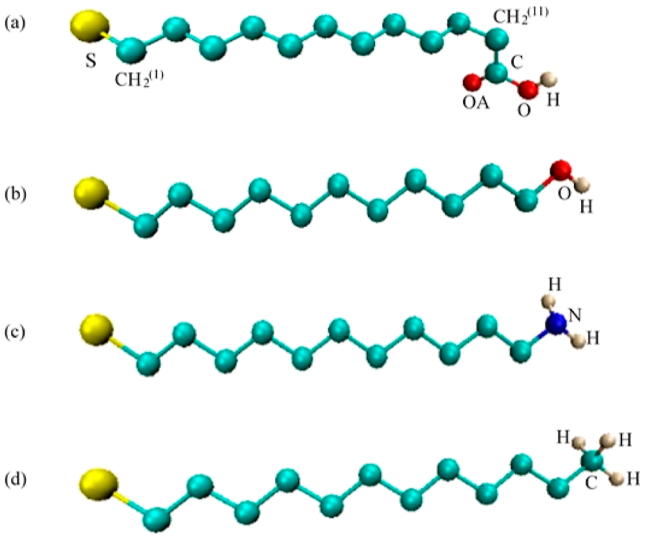

Figure 1. United atom representation of ligand molecules: (a) $-S(CH_2)_{11}COOH$, (b) $-S(CH_2)_{11}OH$, (c) $-S(CH_2)_{11}NH_2$, and (d) $-S(CH_2)_{11}CH_3$. The S atoms are colored yellow, the N atoms are blue, the H atoms are white, the O atoms are red, and the C atoms and CH_2 groups are turquoise.

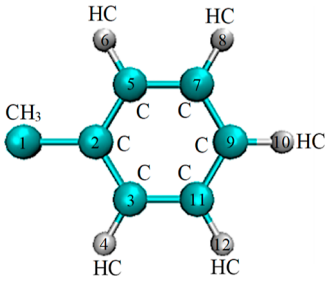

Figure 2. Schematic representation of the model used for toluene molecules.

$$U(r_{ij}) = \sum_{\text{bonds}} \frac{1}{4}k_{ij}^{b}(r_{ij}^2 - b_{ij}^2)^2 + \sum_{\text{angles}} \frac{1}{2}k_{ijk}^{\theta}(\cos(\theta_{ijk}) - \cos(\theta_{ijk}^0))^2 + \sum_{\text{dihedrals}} K_{\psi}(1 + \cos(n\psi - \psi_0) + \sum_{\text{nonbonded}} \left\{ f\frac{q_i q_j}{\varepsilon_r r_{ij}} + 4\epsilon_{ij}\left[\left(\frac{\sigma_{ij}}{r_{ij}}\right)^{12} - \left(\frac{\sigma_{ij}}{r_{ij}}\right)^{6}\right]\right\} \quad (1)$$

where the first and second terms, which are defined as the harmonic potential, indicate the bond stretching and angle bending, respectively. The third term is related to dihedral torsion, and the last two terms correspond to the Coulomb and Lennard-Jones (LJ) potentials, respectively. In this equation, k_{ij}^{b}, k_{ijk}^{θ}, and K_{ψ} are the force constants, r_{ij} is the bond length, and b_{ij} is the reference bond length. θ_{ijk} stands for the angle between the atoms, and θ_{ijk}^0 is the reference value for this angle. Also, ψ is the angle between the ijk and jkl planes, $\psi_0 = 0°$ or 180°, and n is the multiplicity of the torsional dihedral angle. In the last two terms in eq 1, q_i and q_j are the charges of atoms i and j, $f = \frac{1}{4\pi\epsilon_0} = 138.935485$, and ε_r is the relative permittivity. ϵ_{ij} and σ_{ij} are LJ parameters for atoms i and j; that is, ϵ_{ij} represents

https://doi.org/10.1021/acs.jpcb.2c01132
J. Phys. Chem. B 2022, 126, 5534−5543

Table 1. Time Averages of the COM Distance between Each NP Pair ($\overline{d}$) and the Averages of the $\overline{d}$ Values of all NP Pairs ($\overline{d}_{pairs}$) with Standard Deviations

	$\overline{d}$(nm)						
system	1−2	1−3	1−4	2−3	2−4	3−4	$\overline{d}_{pairs}$ (nm)
I	3.31 ± 0.03	4.06 ± 0.04	3.34 ± 0.11	2.96 ± 0.04	3.96 ± 0.04	3.99 ± 0.04	**3.60 ± 0.46**
II	3.96 ± 0.05	4.04 ± 0.08	3.32 ± 0.05	3.15 ± 0.05	4.10 ± 0.08	3.49 ± 0.05	**3.68 ± 0.41**
III	4.04 ± 0.09	3.66 ± 0.14	3.96 ± 0.09	4.09 ± 0.08	3.75 ± 0.08	3.87 ± 0.09	**3.90 ± 0.17**
IV	5.66 ± 0.27	8.49 ± 0.42	6.63 ± 0.33	4.95 ± 0.18	7.44 ± 0.38	6.85 ± 0.14	**6.67 ± 1.26**

the depth of the potential well and σ_{ij} is the finite distance at which the interatomic potential of i and j is zero.

The force-field parameters and electrostatic charges are taken from the previous studies for the terminal groups[57−59] and toluene molecules.[60] The atomic charges of the Au and S atoms and the CH_2 groups are taken as zero. All parameters related to the Au and S atoms are taken from the previous study.[54] The parameters and partial charges belonging to the functional groups in ligand molecules and toluene molecules are listed in the Appendix.

Table 2. Number of H-Bonds between Ligand Molecules of NP Pairs (n_{HB})

system	$n_{HB(ligand-ligand)}$
I	96.18 ± 6.54
II	93.80 ± 4.75
III	44.23 ± 4.79
IV	

Table 3. Diffusion Coefficients of Functionalized Gold NPs

system	$D \times 10^{-7}$ cm^2/s
I	2.06 ± 0.24
II	2.14 ± 0.14
III	2.27 ± 0.20
IV	3.72 ± 0.48

The steepest descent method is used for energy minimization of the systems. The initial system temperature of 2 K is increased to the target temperature by a heating rate of 0.03 K/ps. The temperature is kept constant at 300 K by a v-rescale thermostat with a time constant of 0.1 ps. The pressure is maintained at 1 bar using a Berendsen barostat with a time constant of 0.5 ps and a compressibility of 4.0×10^{-5} bar^{-1} with isotropic coupling. All simulations are performed in the isobaric−isothermal (NPT) ensemble with a 0.5 fs time step by using the leapfrog algorithm. The particle mesh Ewald method is employed for long-range electrostatic interactions. The cutoff distance for LJ and electrostatic interactions is set as 1 nm, and periodic boundary conditions are applied in all directions.

3. RESULTS AND DISCUSSION

All systems are run for a simulation time of 600 ns. By using the Visual Molecular Dynamics program,[61] the snapshot of the initial configuration for system II is taken and it is given as an example in Figure 3; the final configurations of functionalized gold NPs for all systems are given in Figure 4. The S atoms are colored yellow, the N atoms are blue, the H atoms are white, the O atoms are red, the C atoms and CH_2 groups are turquoise, the Au atoms are pink, and the toluene molecules are ochre. After the systems are equilibrated, the calculations are performed for 2 ns simulations by recording MD trajectories more frequently for

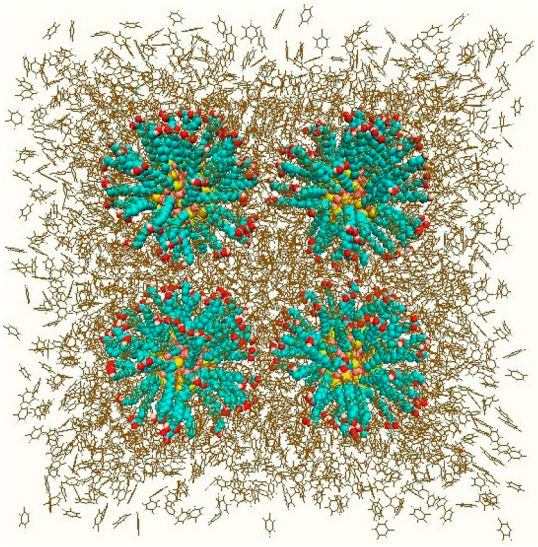

Figure 3. Snapshot of the initial configuration for system II: The gold NPs coated with $SH(CH_2)_{11}OH$ ligand molecules.

analyses. The MD simulation trajectories are saved every 20 ps in the production run, and 1000 frames are collected.

To understand the aggregation/dispersion behaviors of the gold NPs coated by ligand molecules with terminal groups of different polarities in the toluene medium, the center-of-mass (COM) distances between NP pairs are calculated. In addition, the radius of gyration, radial distribution functions (RDFs), mean square displacements (MSDs), diffusion coefficients, and number of H-bonds are computed.

At the beginning of the simulations (t = 0), the positions of NPs are the same for all systems and the average of the COM distance between NP pairs is obtained as approximately 5.68 nm. During the simulation, the COM distance (d) between each NP pair is calculated and the time evaluation of d values is given in Figure 5. As seen in the figure, the d values for systems I, II, and III decrease sharply with time and then remain stable. The decrease in d values indicates that the NPs approach each other and remain stable once these systems reach equilibrium. In Figure 5d, the d values for system IV take values in a large interval, that is, 5−20 nm. This result indicates that NPs are dispersed.

The time average of d values over the last 2 ns of the simulation time ($\overline{d}$) for each NP pair and the average of these values over all NP pairs ($\overline{d}_{pairs}$) are given in Table 1. $\overline{d}_{pairs}$ values for systems I, II, and III are found to be 3.60, 3.68, and 3.90 nm, respectively. All these values are lower than the value of 5.68 nm, which is the average of the COM distance between NP pairs calculated at the beginning of the simulation. The smallest value, 3.60 nm, is found for system I. In this system, gold NPs are coated by the COOH terminal group having the strongest

https://doi.org/10.1021/acs.jpcb.2c01132
J. Phys. Chem. B 2022, 126, 5534−5543

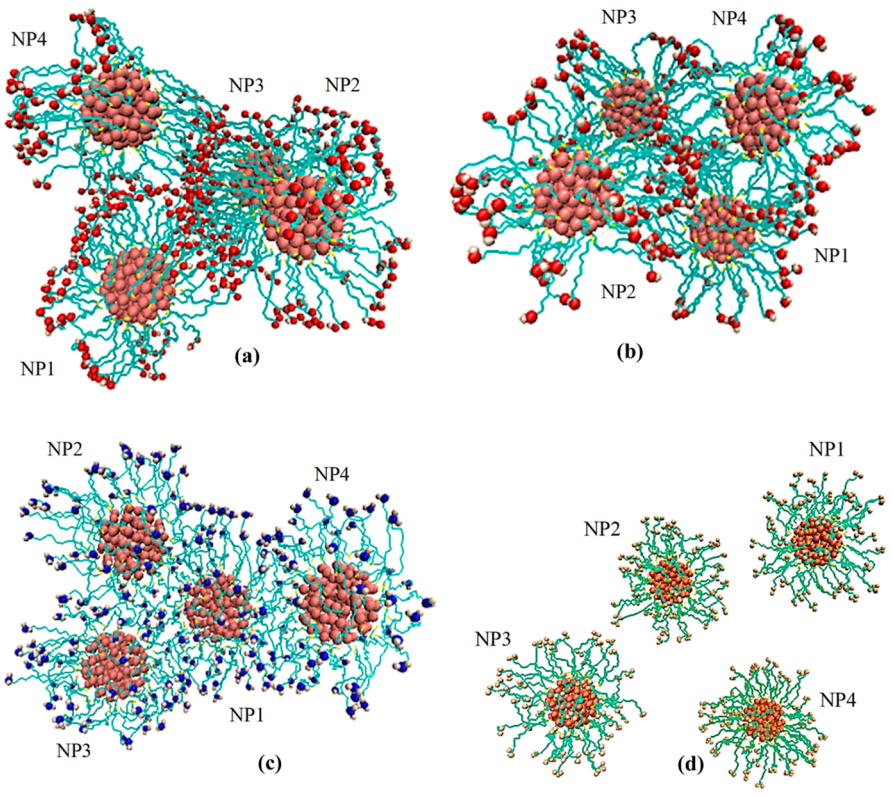

Figure 4. Snapshots of the final configurations of functionalized gold NPs for (a) system I, (b) system II, (c) system III, and (d) system IV. Ligand molecules are $SH(CH_2)_{11}COOH$, $SH(CH_2)_{11}OH$, $SH(CH_2)_{11}NH_2$, and $SH(CH_2)_{11}CH_3$ for these systems, respectively. Alkyl chains are represented as a stick model.

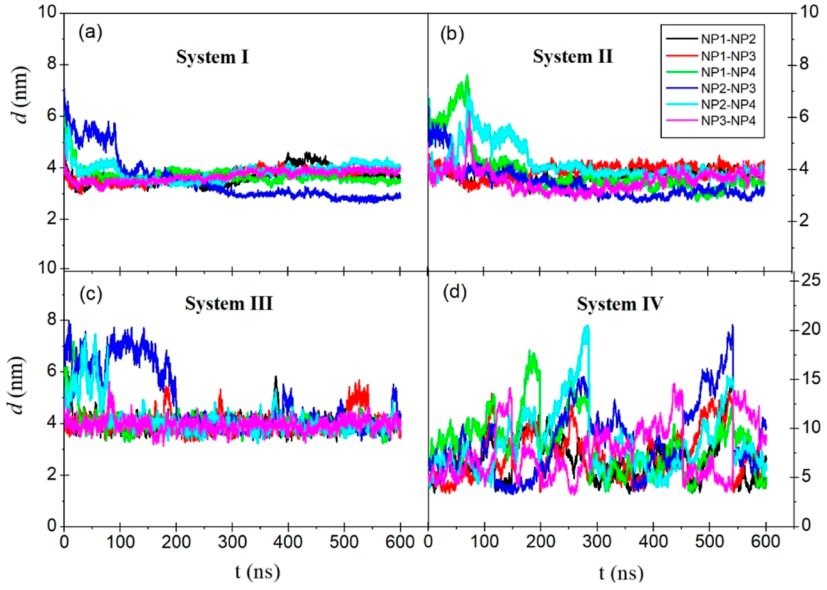

Figure 5. Time evolutions of the COM distances (d) between NP pairs.

polarity in this study. The $\overline{d}_{pairs}$ value increases sequentially for system II and system III, while the polarity of the terminal group of these systems decreases gradually. On the other hand, system IV with a nonpolar CH_3 terminal group has the greatest $\overline{d}_{pairs}$ value, 6.67 nm. This value is greater than the average of the COM distance between NP pairs at the beginning, 5.68 nm. In order to better understand the size of the aggregation and dispersion among these systems, the $\overline{d}_{pairs}$ values with standard deviations are given in Figure 6. While the points under the dotted line correspond to the aggregated systems, the upper point is for the dispersed system.

As seen in the snapshots of the last configuration of the gold NPs with the strongest polar group, that is, COOH, the aggregated four NPs form a spherical cluster pattern (Figure 4a). The aggregation pattern looks more planar for the systems with the OH and NH_2 groups (Figure 4b,c) compared to systems with COOH groups. However, the number of gold NPs in the

https://doi.org/10.1021/acs.jpcb.2c01132
J. Phys. Chem. B 2022, 126, 5534−5543

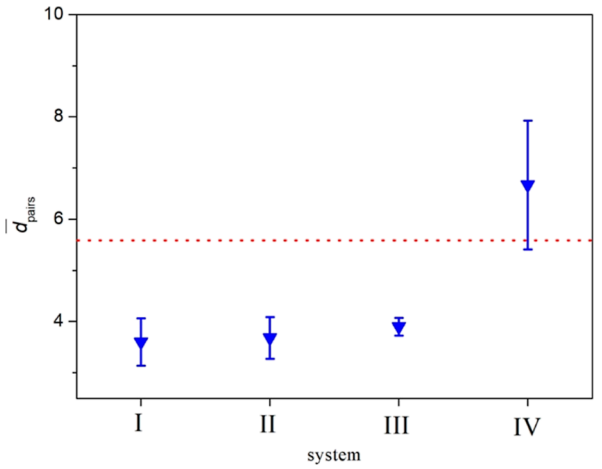

Figure 6. $\overline{d}_{pairs}$ values with standard deviations. The red dotted line shows the average value of the COM distance between NP pairs at the beginning, which is 5.68 nm.

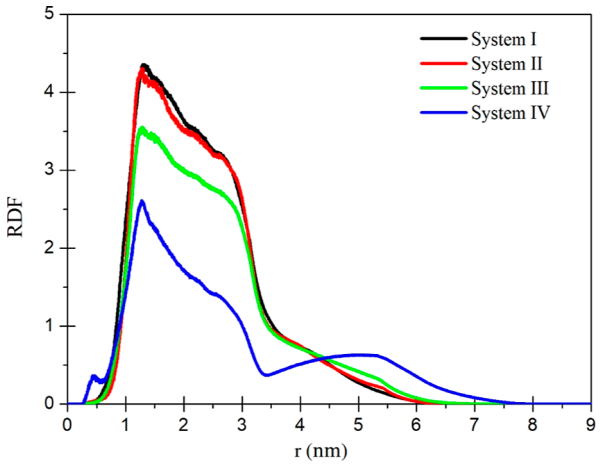

Figure 7. RDFs between the functional group and $CH_2^{(1)}$ united atom in the ligand molecules.

systems is not large enough to make clear comments about the aggregation patterns. In order to obtain more robust results for the aggregation pattern, the number of gold NPs should be increased.

The hydrogen bonds occur between the polar groups in the surface coverage of each gold NP, and the H-bonds also occur between the polar groups of different gold NPs. The H-bond interactions that occurred between the polar groups of different gold NPs are more important in making a comment about the aggregation behavior of NPs, especially in a nonpolar medium such as toluene. Therefore, in this study, the number of H-bonds between the gold NPs is calculated according to the geometric criteria described in the literature.[62] The time averages of H-bond numbers between NP pairs and the standard deviations are given in Table 2. The H-bond occurs only between COOH-, OH-, and NH_2-terminated gold NPs. Therefore, in these systems, the NPs attract each other, and aggregation occurs. For systems I, II, and III, it is observed that the H-bond numbers gradually get smaller by a decrement in the polarity of the functional groups. On the other hand, as a result of the usage of methyl as a functional group, the dispersion of NPs is observed in system IV.

The RDFs between the functional group and the $CH_2^{(1)}$ united atom, which is the first atom bonding with the S atom, in the ligand molecules are calculated by using MD trajectory data corresponding to the last 2 ns of the simulation time, and the results for all systems are given in Figure 7. The $CH_2^{(1)}$ atom is given in Figure 1. As seen in Figure 7, the widths of RDFs for the systems with polar terminal groups are approximately from 0.5 to 6.5 nm. On the other hand, the distribution of system IV with the nonpolar group has a wider width that ends at almost 7.5 nm. While narrow distributions, that is, black, red, and green distributions, for the systems with polar terminal groups are caused by the aggregation of NPs, the wider distribution, namely, the blue distribution, arises from the dispersion of NPs.

The main peak for all systems occurs at nearly 1.4 nm. This value corresponds to the distance between the $CH_2^{(1)}$ atom and the functional group, which is found by using the optimized coordinates of the ligand molecule from quantum mechanical calculations, and also, this value is almost equal to the length of the ligand molecule. Therefore, it can be said that the chains in the ligand molecules are mostly in the all-trans conformation.

To get information about the mobility of functionalized gold NPs in a toluene medium during the first 30 ns (before aggregation/dispersion) and the last 30 ns (after aggregation/dispersion) of the total simulation time, the mean squared displacement of the COM of each NP is calculated and the MSDs for systems I and IV are given as an example in Figures 8

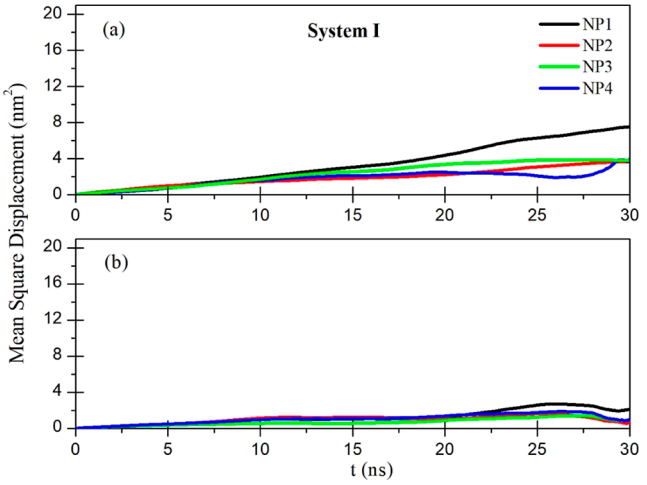

Figure 8. MSDs of functionalized gold NPs with a COOH functional group: (a) first 30 ns and (b) last 30 ns of the simulation time.

and 9, respectively. The slope of these curves corresponds to the diffusion coefficient (D) according to the Einstein relation.[63] When Figure 8a,b is compared, it can be said that in the last 30 ns period, the MSD curves of NPs for system I with the polar COOH terminal group (Figure 8b) are almost parallel to each other because the NPs aggregate and their trajectories are nearly the same. After aggregation, the slopes of the curves become smaller because the mobility of the gold NPs with a polar terminal group is low.

On the other hand, the MSD curve of system IV with a nonpolar CH_3 group during the last 30 ns (Figure 9b) has a much greater slope when it is compared with the curves of the systems with polar terminal groups (Figure 8b). This means that the diffusion coefficients of nonpolar functionalized gold NPs are greater than the value of the polar functionalized gold NPs because the NPs in system IV move more freely. The curves in

https://doi.org/10.1021/acs.jpcb.2c01132
J. Phys. Chem. B 2022, 126, 5534−5543

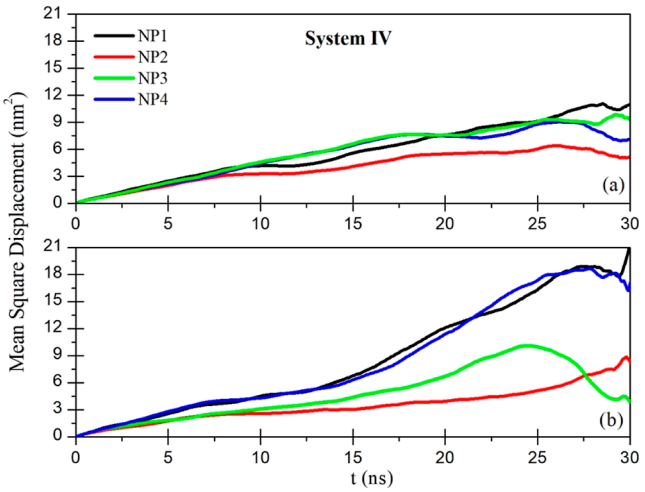

Figure 9. MSDs of functionalized gold NPs with a CH_3 functional group: (a) first 30 ns and (b) last 30 ns of the simulation time.

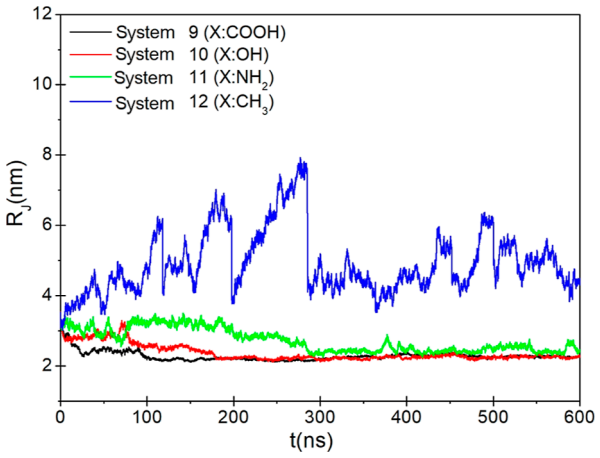

Figure 10. Time evolution of the radius of gyration of gold NPs.

Figure 9b are not parallel to each other because the NPs move away from each other.

The diffusion coefficients for all systems are calculated by using the Einstein relation from the slope of MSD, which is calculated from MD trajectories of 2 ns and given with standard deviations in Table 3.

It can be seen in Table 3 that in the systems with polar terminal groups, the diffusion coefficients of functionalized gold NPs increase with the decrease of the polarity of the terminal groups. The number of H-bonds between terminal groups of the NPs reduces with the decreasing polarity of the terminal groups. When the H-bond number decreases, the mobility of NPs increases, and therefore, the diffusion coefficient increases. The NPs with a nonpolar CH_3 group can move freely because there is no H-bond interaction between them. Therefore, the highest diffusion coefficient is obtained for this system.

In order to evaluate the size of the aggregate of four functionalized gold NPs, the radius of gyration is calculated by using the following equation

$$R_g = \left(\frac{\sum_i \|r_i\|^2 m_i}{\sum_i m_i} \right)^{1/2} \quad (2)$$

where m_i is the mass of atom i and r_i is the distance of atom i from the COM. Figure 10 shows the time evolution of the radius of gyration (R_g). As can be seen in the figure, the initial value of R_g is almost 3 nm for all systems. While the radius of gyration decreases with the increasing simulation time for the systems with polar terminal groups, it has larger values for the system with a nonpolar methyl group. Smaller R_g values than the initial value indicate that the NPs get closer to each other; meanwhile, the larger values indicate that the NPs move away from each other.

4. CONCLUSIONS

In this study, the effect of the polarity of the terminal group on the aggregation of the gold NPs coated with the dodecanethiol ligand molecules in a liquid toluene environment is investigated by using atomistic MD simulation. The terminal group of dodecanethiol ligand molecules is changed to carboxyl, hydroxyl, amine, and methyl groups. The presence of polar functional groups in the ligand molecules of NPs creates attractive interaction contributions at long ranges and causes the H-bonds between the NPs, which are a specific type of dipole−dipole interaction. On the other hand, there is no strong attractive interaction between the NPs with the methyl group because the alkanes are nonpolar, and they interact by means of weak forces. Therefore, the gold NPs with the nonpolar methyl group move independently in the toluene solvent and they do not exhibit aggregation behavior. Calculations indicate that the polar carboxyl-, hydroxyl-, and amine-terminated gold NPs aggregate in the nonpolar toluene solvent, whereas the nonpolar methyl-terminated gold NPs disperse. This result agrees with the previous work[34] with the butane nonpolar solvent.

Because the electronegativity difference in the COOH, OH, and NH_2 functional groups gradually decreases, the H-bond interactions between the NPs covered with these functional groups weaken, so the size of aggregation gradually reduces. Consequently, an increment in the polarity of the functional groups causes a decrement in the size of the aggregate of functionalized gold NPs. The smallest size of aggregates is obtained in the system with the carboxyl terminal group. The slopes of the MSD curves show that the diffusion coefficients have small values for the gold NPs with polar terminal groups because their mobilities are limited due to their aggregation. The diffusion coefficients increase with the decrease of the polarity of the terminal groups. On the other hand, the diffusion coefficient has the highest value for the gold NPs with the methyl terminal group because they move more freely. Calculation of the radius of gyration supports the result that the gold NPs with polar terminal groups aggregate and the gold NPs with nonpolar terminal groups disperse.

The obtained aggregation/dispersion behaviors of functionalized gold NPs in this study with the nonpolar toluene solvent are exactly contrary to the behaviors of functionalized gold NPs in previous studies in a polar water solvent.[34,46] It is found that hydrophobic CH_3 terminal groups lead to the aggregation of gold NPs in a water medium. On the other hand, the aggregation of gold NPs with polar hydroxyl groups is weakened because of the attractive interactions between solvent molecules and terminal groups.[46]

In this study, due to the nonpolar toluene solvent medium, all gold NPs with a polar functional group attract each other, and as a result of this behavior, the aggregation is strong. If the solvent was polar, the polar functional group in ligand molecules would mostly interact with polar solvent molecules nearest to them. In this scenario, the H-bonds would probably occur mostly

https://doi.org/10.1021/acs.jpcb.2c01132
J. Phys. Chem. B 2022, 126, 5534−5543

Table 4. GROMOS Force-Field Parameters for COOH, OH, NH_2, and CH_3 Groups in Ligand Molecules

functional group	atom	mass (amu)	q(e)	functional group	atom	mass (amu)	q(e)
COOH	C	12.011	+0.530	CH_3	C	12.011	−0.180
	OA	15.999	−0.380		H	1.008	+0.060
	O	15.999	−0.548		H	1.008	+0.060
	H	1.008	0.398		H	1.008	+0.060
OH	CH_2[11]	14.027	+0.150	NH_2	NT	14.007	−0.830
	O	15.999	−0.548		H	1.008	+0.415
	H	1.008	0.398		H	1.008	+0.415

bond	r_{eq} (nm)	k_r (kJmol^{-1} nm^4) × 10^6
CH_2−O	0.143	8.18
C−O	0.136	10.20
C═OA	0.123	16.60
O−H	0.100	15.70
CH_2−N	0.147	8.71
N−H	0.100	18.70
CH_2−C	0.153	7.15
C−H	0.109	12.30

angle	θ_{eq} (deg)	k_θ (kJmol^{-1})
C−O−H	109.5	450.00
CH_2−CH_2−O	111	530.00
CH_2−C=OA	125	750.00
O−C═OA	122	700.00
H−N−H	109.5	380.00
CH_2−CH_2−N	111	530.00
CH_2−N−H	109.5	425.00
CH_2−C−H	109.5	292.88
H−C−H	107.8	276.14

torsion	Ψ	C_n (kJmol^{-1})	n
CH_2−CH_2−O−H	0	1.26	3
CH_2−CH_2−CH_2−O	0	5.92	3
CH_2−CH_2−C−O	0	1.00	6
CH_2−CH_2−C═OA	0	1.00	6
CH_2−C−O−H	180	16.70	2
OA═C−O−H	180	16.70	2
CH_2−CH_2−C−H	0	1.00	6
CH_2−CH_2−CH_2−C	0	5.92	3
CH_2−CH_2−N−H	0	3.77	6
CH_2−CH_2−CH_2−N	0	3.77	6
CH_2−CH_2−CH_2−CH_2	0	5.92	3

between the polar functional groups and polar solvent molecules, so the aggregation would not be strong. To make a more detailed comment on the behavior of these gold NPs in polar solvents, we are planning to investigate their behaviors in water in our future study.

As the results obtained in this study present that the aggregation/dispersion behavior of functionalized gold NPs can be controlled by changing the polarity of terminal groups of coated ligand molecules, they have great application potential in diverse fields that requires a better understanding of these behaviors of functionalized gold NPs. Therefore, these observations are thought to contribute to future studies based on the aggregation/dispersion behavior of functionalized gold NPs in nonpolar liquids.

APPENDIX

GROMOS force-field parameters for terminal groups were used in the calculations [see eq 1 and Tables 4 and 5].

AUTHOR INFORMATION

Corresponding Author

Ayse Cetin − *Department of Physics, Faculty of Science, Ege University, Izmir 35100, Turkey;* orcid.org/0000-0002-9923-6210; Email: akafali84@hotmail.com

Author

Mine Ilk Capar − *Department of Physics, Faculty of Science, Ege University, Izmir 35100, Turkey*

Complete contact information is available at: https://pubs.acs.org/10.1021/acs.jpcb.2c01132

Notes

The authors declare no competing financial interest.

ACKNOWLEDGMENTS

This work has been supported by TUBITAK (Turkish Agency) under Research Project number 117F246. The numerical calculations reported in this paper were fully performed at the

Table 5. GROMOS Force-Field Parameters for Toluene Molecules

atom type	mass (amu)	q(e)
$^{1}CH_3$	15.035	−0.076
^{2}C	12.011	+0.290
^{3}C	12.011	−0.260
^{4}HC	1.008	0.142
^{5}C	12.011	−0.260
^{6}HC	1.008	0.142
^{7}C	12.011	−0.100
^{8}HC	1.008	0.122
^{9}C	12.011	−0.157
^{10}HC	1.008	0.135
^{11}C	12.011	−0.100
^{12}HC	1.008	0.122
bond	r_{eq} (nm)	k_r (kJmol^{-1} nm^{4}) × 10^{6}
$^{1}CH_3$–^{2}C	0.152	5.43
^{2}C–^{3}C	0.140	8.54
^{2}C–^{5}C	0.140	8.54
^{3}C–^{4}HC	0.109	12.30
^{3}C–^{11}C	0.139	8.66
^{5}C–^{6}HC	0.109	12.30
^{5}C–^{7}C	0.139	8.66
^{7}C–^{8}HC	0.109	12.30
^{7}C–^{9}C	0.139	8.66
^{9}C–^{10}HC	0.109	12.30
^{9}C–^{11}C	0.139	8.66
^{11}C–^{12}HC	0.109	12.30
angle	θ_{eq} (deg)	k_θ (kJmol^{-1})
$^{1}CH_3$–^{2}C–^{3}C	120	560
$^{1}CH_3$–^{2}C–^{5}C	120	560
^{3}C–^{2}C–^{5}C	120	560
^{2}C–^{3}C–^{4}HC	120	505
^{2}C–^{3}C–^{11}C	120	560
^{4}HC –^{3}C–^{11}C	120	505
^{2}C–^{5}C–^{6}HC	120	505
^{2}C–^{5}C–^{7}C	120	560
^{6}HC–^{5}C–^{7}C	120	505
^{5}C–^{7}C–^{8}HC	120	505
^{5}C–^{7}C–^{9}C	120	560
^{8}HC–^{7}C–^{9}C	120	505
^{7}C–^{9}C–^{10}HC	120	505
^{7}C–^{9}C–^{11}C	120	560
^{10}HC–^{9}C–^{11}C	120	505
^{3}C–^{11}C–^{9}C	120	560
^{3}C–^{11}C–^{12}HC	120	505
^{9}C–^{11}C–^{12}HC	120	505
torsion	Ψ	C_n (kJmol^{-1})	n
^{5}C–^{2}C–^{3}C–^{11}C	180	41.8	2
^{3}C–^{2}C–^{5}C–^{7}C	180	41.8	2
^{2}C–^{3}C–^{11}C–^{9}C	180	41.8	2
^{2}C–^{5}C–^{7}C–^{9}C	180	41.8	2
^{5}C–^{7}C–^{9}C–^{11}C	180	41.8	2
^{7}C–^{9}C–^{11}C–^{3}C	180	41.8	2

TUBITAK ULAKBIM, High Performance and Grid Computing Center (TRUBA resources).

REFERENCES

(1) Schmid, G.; Fenske, D. Metal Clusters and Nanoparticles. *Philos. Trans. R. Soc., A* **2010**, *368*, 1207−1210.
(2) Geonmonond, R. S.; Silva, A. G. M.; Camargo, P. H. C. Controlled Synthesis of Noble Metal Nanomaterials: Motivation, Principles, and Opportunities in Nanocatalysis. *An. Acad. Bras. Cienc.* **2018**, *90*, 719−744.
(3) Jain, P. K.; Huang, X.; El-Sayed, I. H.; El-Sayed, M. A. Noble Metals on the Nanoscale: Optical and Photothermal Properties and Some Applications in Imaging, Sensing, Biology, and Medicine. *Acc. Chem. Res.* **2008**, *41*, 1578−1586.
(4) Huang, X.; El-Sayed, M. A. Gold Nanoparticles: Optical Properties and Implementations in Cancer Diagnosis and Photothermal Therapy. *J. Adv. Res.* **2010**, *1*, 13−28.
(5) Dykman, L. A.; Khlebtsov, N. G. Gold Nanoparticles in Biology and Medicine: Recent Advances and Prospects. *Acta Naturae* **2011**, *3*, 34−55.
(6) Daraee, H.; Eatemadi, A.; Abbasi, E.; Fekri Aval, S. F.; Kouhi, M.; Akbarzadeh, A. Application of Gold Nanoparticles in Biomedical and Drug Delivery. *Artif. Cells, Nanomed., Biotechnol.* **2016**, *44*, 410−422.
(7) Murali, K.; Neelakandan, M. S.; Thomas, S. Biomedical Applications of Gold Nanoparticles. *JSM. Nanotechnol. Nanomed.* **2018**, *6*, 1064.
(8) Yang, Y.; Wang, L.; Wan, B.; Gu, Y.; Li, X. Optically Active Nanomaterials for Bioimaging and Targeted Therapy. *Front. Bioeng. Biotechnol.* **2019**, *7*, 320.
(9) Mugaka, B. P.; Hu, Y.; Ma, Y.; Ding, Y. *Surface Modification of Gold Nanoparticles for Targeted Drug Delivery*; Pathak, Y. V., Ed.; Springer: Cham, 2019; pp 391−403.
(10) Amina, S. J.; Guo, B. A Review on the Synthesis and Functionalization of Gold Nanoparticles as a Drug Delivery Vehicle. *Int. J. Nanomed.* **2020**, *15*, 9823−9857.
(11) Sperling, R. A.; Parak, W. J. Surface Modification, Functionalization and Bioconjugation of Colloidal Inorganic Nanoparticles. *Philos. Trans. R. Soc., A* **2010**, *368*, 1333−1383.
(12) Giljohann, D. A.; Seferos, D. S.; Daniel, W. L.; Massich, M. D.; Patel, P. C.; Mirkin, C. A. Gold Nanoparticles for Biology and Medicine. *Angew. Chem., Int. Ed. Engl.* **2010**, *49*, 3280−3294.
(13) Fratoddi, I.; Venditti, I.; Cametti, C.; Russo, M. V. Gold Nanoparticles and Gold Nanoparticle Conjugates for Delivery of Therapeutic Molecules. Progress and Challenges. *J. Mater. Chem. B* **2014**, *2*, 4204−4220.
(14) Fratoddi, I. Hydrophobic and Hydrophilic Au and Ag Nanoparticles. Breakthroughs and Perspectives. *Nanomaterials* **2017**, *8*, 11.
(15) Kim, T.; Lee, C. H.; Joo, S. W.; Lee, K. Kinetics of Gold Nanoparticle Aggregation: Experiments and Modeling. *J. Colloid Interface Sci.* **2008**, *318*, 238−243.
(16) Chegel, V.; Rachkov, O.; Lopatynskyi, A.; Ishihara, S.; Yanchuk, I.; Nemoto, Y.; Hill, J. P.; Ariga, K. Gold Nanoparticles Aggregation: Drastic Effect of Cooperative Functionalities in a Single Molecular Conjugate. *J. Phys. Chem. C* **2012**, *116*, 2683−2690.
(17) Wang, S. H.; Lee, C. W.; Chiou, A.; Wei, P. K. Size-dependent Endocytosis of Gold Nanoparticles Studied by Three-Dimensional Mapping of Plasmonic Scattering Images. *J. Nanobiotechnol.* **2010**, *8*, 33.
(18) Pluchery, O.; Remita, H.; Schaming, D. Demonstrative Experiments about Gold Nanoparticles and Nanofilms: an Introduction to Nanoscience. *Gold Bull.* **2013**, *46*, 319−327.
(19) Pamies, R.; Cifre, J. G. H.; Espín, V. F.; Collado-González, M.; Baños, F. G. D.; de la Torre, J. G. Aggregation Behaviour of Gold Nanoparticles in Saline Aqueous Media. *J. Nanopart. Res.* **2014**, *16*, 2376.
(20) Parboosing, R.; Govender, T.; Maguire, G. E. M.; Kruger, H. G. Synthesis Characterization and Biocompatibility of a Multifunctional Gold Nanoparticle System for the Delivery of Single-Stranded RNA to Lymphocytes. *S. Afr. J. Chem.* **2018**, *71*, 1−14.

https://doi.org/10.1021/acs.jpcb.2c01132
J. Phys. Chem. B 2022, 126, 5534−5543

(21) Singh, K.; Raghav, A.; Jha, P. K.; Satapathi, S. Effect of Size and Charge Asymmetry on Aggregation Kinetics of Oppositely Charged Nanoparticles. *Sci. Rep.* **2019**, *9*, 3762.
(22) Hwang, S. H.; Jeong, S.; Choi, H. J.; Eun, H.; Jo, M. G.; Kwon, W. Y.; Kim, S.; Kim, Y.; Lee, M.; Park, K. S. Target-Induced Aggregation of Gold Nanoparticles for Colorimetric Detection of Bisphenol A. *J. Nanomater.* **2019**, *2019*, 3676384.
(23) Cordray, M. S.; Amdahl, M.; Richards-Kortum, R. R. Gold Nanoparticle Aggregation for Quantification of Oligonucleotides: Optimization and Increased Dynamic Range. *Anal. Biochem.* **2012**, *431*, 99−105.
(24) Deffner, M.; Schulz, F.; Lange, H. Impact of the Crosslinker's Molecular Structure on the Aggregation of Gold Nanoparticles. *Z. Phys. Chem.* **2017**, *231*, 19−31.
(25) Stein, B.; Zopes, D.; Schmudde, M.; Schneider, R.; Mohsen, A.; Goroncy, C.; Mathur, S.; Graf, C. Kinetics of Aggregation and Growth Processes of PEG-Stabilised Mono- and Multivalent Gold Nanoparticles in Highly Concentrated Halide Solutions. *Faraday Discuss.* **2015**, *181*, 85−102.
(26) Li, R.; Gu, X.; Liang, X.; Hou, S.; Hu, D. Aggregation of Gold Nanoparticles Caused in Two Different Ways Involved in 4-Mercaptophenylboronic Acidand Hydrogen Peroxide. *Materials* **2019**, *12*, 1802.
(27) Isnaeni; Irmaniar; Herbani, Y. Aggregation Effect on Absorbance Spectrum of Laser Ablated Gold Nanoparticles. *J. Phys.: Conf. Ser.* **2017**, *817*, 012039.
(28) Zhou, W.; Hu, K.; Kwee, S.; Tang, L.; Wang, Z.; Xia, J.; Li, X. J. Gold Nanoparticle Aggregation-Induced Quantitative Photothermal Biosensing Using a Thermometer: A Simple and Universal Biosensing Platform. *Anal. Chem.* **2020**, *92*, 2739−2747.
(29) Balasubramanian, R.; Xu, J.; Kim, B.; Sadtler, B.; Wei, A. Extraction and Dispersion of Large Gold Nanoparticles in Nonpolar Solvents. *J. Dispersion Sci. Technol.* **2001**, *22*, 485−489.
(30) Hamamoto, M.; Liang, Y.; Yagyu, H. Synthesis of Gold Nanoparticles Dispersion in Toluene Using Immiscible Fluid Flow in Microfluidic Device. *Electron Commun. Jpn.* **2019**, *102*, 48−54.
(31) Sadrolhosseini, A. R.; Rashid, S. A.; Zakaria, A. Synthesis of Gold Nanoparticles Dispersed in Palm Oil Using Laser Ablation Technique. *J. Nanomater.* **2017**, *2017*, 6496390.
(32) Kyrychenko, A.; Karpushina, G. V.; Bogatyrenko, S. I.; Kryshtal, A. P.; Doroshenko, A. O. Preparation, Structure, and a Coarse-Grained Molecular Dynamics Model for Dodecanethiol-Stabilized Gold Nanoparticles. *Comput. Theor. Chem.* **2011**, *977*, 34−39.
(33) Lal, M.; Plummer, M.; Purton, J.; Smith, W. A Computer Simulation Study of the Interaction between Passivated and Bare Gold Nanoclusters. *Proc. R. Soc. A* **2011**, *467*, 1986−2003.
(34) Lin, J. Q.; Zhang, H. W.; Chen, Z.; Zheng, Y. G.; Zhang, Z. Q.; Ye, H.-F. Simulation Study of Aggregations of Monolayer-Protected Gold Nanoparticles in Solvents. *J. Phys. Chem. C* **2011**, *115*, 18991−18998.
(35) Jabes, B. S.; Yadav, H. O. S.; Kumar, S. K.; Chakravarty, C. Fluctuation-Driven Anisotropy in Effective Pair Interactions between Nanoparticles: Thiolated Gold Nanoparticles in Ethane. *J. Chem. Phys.* **2014**, *141*, 154904.
(36) Cheng, L.; Cao, D. Aggregation of Polymer-Grafted Nanoparticles in Good Solvents: A Hierarchical Modeling Method. *J. Chem. Phys.* **2011**, *135*, 124703.
(37) Slyusarchuk, A. Y.; Yaremchuk, D. L.; Yaremchuk, J. M.; Ilnytskyi, J. M. Adsorption of Decorated Nanoparticles on a Liquid Crystalline Polymer Brush: Molecular Dynamics Study. *Math. Model. Comput.* **2020**, *7*, 207−218.
(38) Zhang, X.; Lin, W.; Wen, L.; Yao, N.; Nie, S.; Zhang, L. Systematic Design and Application of Unimolecular Star-Like Block Copolymer Micelles: A Coarse-Grained Simulation Study. *Phys. Chem. Chem. Phys.* **2016**, *18*, 26519−26529.
(39) Munaò, G.; Correa, A.; Pizzirusso, A.; Milano, G. On the Calculation of the Potential of Mean Force between Atomistic Nanoparticles. *Eur. Phys. J. E* **2018**, *41*, 38.
(40) Sridhar, D. B.; Gupta, R.; Rai, B. Effect of Surface Coverage and Chemistry on Self-Assembly of Monolayer Protected Gold Nanoparticles: A Molecular Dynamics Simulation Study. *Phys. Chem. Chem. Phys.* **2018**, *20*, 25883−25891.
(41) Brancolini, G.; Lopez, H.; Corni, S.; Tozzini, V. Low-Resolution Models for the Interaction Dynamics of Coated Gold Nanoparticles with β2-microglobulin. *Int. J. Mol. Sci.* **2019**, *20*, 3866.
(42) Lunnoo, T.; Assawakhajornsak, J.; Puangmali, T. In Silico Study of Gold Nanoparticle Uptake into a Mammalian Cell: Interplay of Size, Shape, Surface Charge, and Aggregation. *J. Phys. Chem. C* **2019**, *123*, 3801−3810.
(43) Shen, Z.; Baker, W.; Ye, H.; Li, Y. pH-Dependent Aggregation and pH-Independent Cell Membrane Adhesion of Monolayer-Protected Mixed Charged Gold Nanoparticles. *Nanoscale* **2019**, *11*, 7371.
(44) Van Lehn, R. C.; Alexander-Katz, A. Ligand-Mediated Short-Range Attraction Drives Aggregation of Charged Monolayer-Protected Gold Nanoparticles. *Langmuir* **2013**, *29*, 8788−8798.
(45) Cui, M.; Yang, X. Molecular Simulation of Gold Nanoparticle Dispersion and Aggregation in Supercritical CO2. *J. Mater. Sci.* **2013**, *48*, 891−899.
(46) Devi, J. M. Aggregation of Thiol Coated Gold Nanoparticles: A Simulation Study on the Effect of Polymer Coverage Density and Solvent. *Comput. Mater. Sci.* **2014**, *86*, 174−179.
(47) Lane, J. M. D.; Grest, G. S. Assembly of Responsive-Shape Coated Nanoparticles at Water Surfaces. *Nanoscale* **2014**, *6*, 5132−5137.
(48) Villarreal, O. D.; Chen, L. Y.; Whetten, R. L.; Yacaman, M. J. Ligand-Modulated Interactions between Charged Monolayer-Protected Au144(Sr)60 Gold Nanoparticles in Physiological Saline. *Phys. Chem. Chem. Phys.* **2015**, *17*, 3680−3688.
(49) Villarreal, O. D.; Chen, L. Y.; Whetten, R. L.; Demeler, B. Aspheric Solute Ions Modulate Gold Nanoparticle Interactions in an Aqueous Solution: An Optimal Way to Reversibly Concentrate Functionalized Nanoparticles. *J. Phys. Chem. B* **2015**, *119*, 15502−15508.
(50) Salerno, K. M.; Bolintineanu, D. S.; Lane, J. M. D.; Grest, G. S. Ligand Structure and Mechanical Properties of Single-Nanoparticle-Thick Membranes. *Phys. Rev. E* **2015**, *91*, 062403.
(51) Khavani, M.; Izadyar, M.; Housaindokht, M. R. Modeling of the Functionalized Gold Nanoparticle Aggregation in the Presence of Dopamine: A Joint MD/QM Study. *J. Phys. Chem. C* **2018**, *122*, 26130−26141.
(52) Van Der Spoel, D.; Lindahl, E.; Hess, B.; Groenhof, G.; Mark, A. E.; Berendsen, H. J. C. GROMACS: Fast, Flexible and Free. *J. Comput. Chem.* **2005**, *26*, 1701−1718.
(53) Martínez, L.; Andrade, R.; Birgin, E. G.; Martínez, J. M. PACKMOL: A Package for Building Initial Configurations for Molecular Dynamics Simulations. *J. Comput. Chem.* **2009**, *30*, 2157−2164.
(54) Heikkilä, E.; Gurtovenko, A. A.; Martinez-Seara, H.; Häkkinen, H.; Vattulainen, I.; Akola, J. Atomistic Simulations of Functional Au144(SR)60 Gold Nanoparticles in Aqueous Environment. *J. Phys. Chem. C* **2012**, *116*, 9805−9815.
(55) Kashiwagi, H.; Hashimoto, T.; Tanaka, Y.; Kubota, H.; Makita, T. Thermal Conductivity and Density of Toluene in The Temperature Range 273-373 K at Pressures up to 250 MPa. *Int. J. Thermophys.* **1982**, *3*, 201−215.
(56) Oostenbrink, C.; Villa, A.; Mark, A. E.; Van Gunsteren, W. F. A Biomolecular Force Field Based on The Free Enthalpy of Hydration and Solvation: The GROMOS Force-Field Parameter Sets 53A5 and 53A6. *J. Comput. Chem.* **2004**, *25*, 1656−1676.
(57) Horta, B. A. C.; Fuchs, P. F. J.; van Gunsteren, W. F.; Hünenberger, P. H. New Interaction Parameters for Oxygen Compounds in The GROMOS Force Field: Improved Pure-Liquid and Solvation Properties for Alcohols, Ethers, Aldehydes, Ketones, Carboxylic Acids, and Esters. *J. Chem. Theory Comput.* **2011**, *7*, 1016−1031.
(58) Lemkul, J. A.; Allen, W. J.; Bevan, D. R. Practical Considerations for Building GROMOS-Compatible Small-Molecule Topologies. *J. Chem. Inf. Model.* **2010**, *50*, 2221−2235.

https://doi.org/10.1021/acs.jpcb.2c01132
J. Phys. Chem. B 2022, 126, 5534−5543

(59) Raut, V. P.; Agashe, M. A.; Stuart, S. J.; Latour, R. A. Molecular Dynamics Simulations of Peptide-Surface Interactions. *Langmuir* **2005**, *21*, 1629−1639.
(60) Malde, A. K.; Zuo, L.; Breeze, M.; Stroet, M.; Poger, D.; Nair, P. C.; Oostenbrink, C.; Mark, A. E. An Automated Force Field Topology Builder (ATB) And Repository: Version 1.0. *J. Chem. Theory Comput.* **2011**, *7*, 4026−4037.
(61) Humphrey, W.; Dalke, A.; Schulten, K. VMD: Visual Molecular Dynamics. *J. Mol. Graphics* **1996**, *14*, 33−38.
(62) Luzar, A.; Chandler, D. Hydrogen-Bond Kinetics in Liquid Water. *Nature* **1996**, *379*, 55−57.
(63) Cetin, A.; Capar, M. I.; Zakharov, A. V. Miscibility and Diffusivity of Water in Organic Acids: Molecular Dynamics Simulations. *J. Mol. Liq.* **2019**, *294*, 111630.

https://doi.org/10.1021/acs.jpcb.2c01132
J. Phys. Chem. B 2022, 126, 5534−5543